communications physics

A Nature Portfolio journal

Article

https://doi.org/10.1038/s42005-026-02496-9

Non-Hermitian skin effect without point-gap topology in 2D quasicrystals

Xiaoming Cai

The non-Hermitian skin effect refers to the accumulation of an extensive number of eigenstates at the boundaries of particular dissipative systems. This phenomenon has sparked widespread interest across various fields of physics. It has been dramatically improving our understanding of non-Hermitian systems and paving the way for new opportunities in fundamental and applied research of topological phenomena. It is generally believed to be associated with a nontrivial point-gap spectral topology. Nevertheless, we report observing the non-Hermitian skin effect without point-gap topology in the two-dimensional nonreciprocal Hofstadter model subjected to an incommensurate magnetic field- a quasicrystal. Under periodic boundary conditions, the spectrum is real without point-gap topology but has significant degeneracy. However, when open boundary conditions are applied, eigenstates are exponentially localized at edges, showing the non-Hermitian skin effect, and the degeneracy is broken. This degeneracy-breaking-induced non-Hermitian skin effect results in anomalous wave packet dynamics.

Exploration of non-Hermitian physics has flourished in the last few years[1–3]. It covers a wide range of classical wave systems such as lossy acoustic cavities[4–8] or photonic crystals[8–15], open quantum systems connected to the environment[16–18], and quasiparticles with finite lifetimes in condensed matter[19,20]. Complex features, including non-real eigenvalues[21], non-orthogonal eigenvectors[22,23], and exceptional points[24,25] are characteristics of non-Hermitian systems. They give rise to a variety of intrinsic phenomena without parallels in the Hermitian limit. A prime example is the non-Hermitian skin effect (NHSE)[26–29], the anomalous localization of extensive bulk states at the open boundaries. Numerous platforms have witnessed the effective observation of NHSE. Its potential applications, including unidirectional amplifiers[30], optical funnels[31], high-efficiency energy harvesting[32], and enhanced sensors[33–35], also have been explored.

In NHSE, extensive boundary-localized bulk states lead to the failure of traditional Bloch band theory and the breakdown of conventional bulk-boundary correspondence[36]. These motivate the novel concept of the generalized Brillouin zone, formed by introducing an imaginary part to the Bloch wave vector to account for the exponentially localized skin states[37]. In dynamics, NHSE manifests as the nonreciprocal propagation of the wave packet, which suppresses the entanglement propagation and thermalization[38]. At the heart of the NHSE lies the point-gap topology of the energy spectrum under the periodic boundary condition (PBC). In one dimension (1D), the eigenvalues under PBC can form a closed curve on the complex energy plane, deviating from a specific reference point, i.e., point gap. Then, a spectral winding number can be defined with respect to the reference point. The necessary and sufficient condition for the presence of NHSE is the non-zero spectral winding number or nontrivial point-gap topology[39]. When there are higher dimensions, displaying more possible symmetries and geometries, NHSE will have richer connotations and be the subject of debate[40–42]. It has been suggested that a global criterion connects the spectral area to the occurrence of NHSE[43]. In this case, corresponding eigenenergies under PBC form a closed curve with nontrivial point-gap topology, as the Bloch wave vector, perpendicular to the open boundary which hosts skin states, goes through the Brillouin zone.

In this paper, we report the NHSE outside the framework of the point-gap topology in 2D quasicrystals. We consider a 2D anisotropic square lattice with nonreciprocal hoppings in one direction, say the y dimension, and an incommensurate magnetic field penetrating the lattice. Under PBCs, the incommensurate magnetic field can induce Anderson localization of states in the y dimension, eliminating effects of the nonreciprocity on spectra. The spectrum is real, with zero winding numbers. However, the system possesses huge degeneracy. On the other side, under open boundary conditions (OBCs), the open boundary in the x dimension causes degeneracy breaking. Degenerated y-dimension-localized states superpose to form extended states, which turn into skin states in the presence of nonreciprocal hoppings. The degeneracy-breaking-induced NHSE manifests in dynamics as an anomalous nonreciprocal propagation of the wave packet.

Innovation Academy for Precision Measurement Science and Technology, Chinese Academy of Sciences, Wuhan, China.
e-mail: cxmpx@wipm.ac.cn

Results and Discussion

Nonreciprocal Hofstadter model

Our exploration of the anomalous NHSE commences with a single particle within a nonreciprocal square lattice, subjected to a vertical uniform magnetic field. It is described by the nonreciprocal Hofstadter model, which is written as

$$H = \sum_{n,m}\Big(t_x c^\dagger_{n+1,m}c_{n,m} + t_x c^\dagger_{n,m}c_{n+1,m} + t_y e^{i2\pi\beta n+g} c^\dagger_{n,m+1}c_{n,m} + t_y e^{-i2\pi\beta n-g} c^\dagger_{n,m}c_{n,m+1}\Big). \quad (1)$$

$c^\dagger_{n,m}$ ($c_{n,m}$) is the creation (annihilation) operator at the lattice site (n, m). t_x represents the nearest-neighbor hopping amplitude in the x direction. t_y is the geometric average of the nonreciprocal hopping amplitudes in the y direction, and g characterizes the strength of nonreciprocity. The phase factor β is defined by the magnetic flux through a lattice cell (lattice constant 1). In the presence of a homogeneous magnetic field, the Hofstadter model has a magnetic translation group and an enlarged magnetic unit cell[44]. Above, the Landau gauge $\mathbf{A} = (0, \beta n)$ has been adopted. We focus on the situation that β is an irrational number like the golden ratio $(\sqrt{5}-1)/2$, which makes the model quasiperiodic. The quasiperiodicity is the source of all phenomena and makes the model distinguishable from others[45,46]. In practice, the irrational $\beta = (\sqrt{5}-1)/2$ is approximated by rational numbers $\beta = F_l/F_{l+1}$ with F_l the lth Fibonacci number[47]. Correspondingly, the total number of lattice sites is $L \times L$ with the linear size $L = F_{l+1}$. Without loss of generality, we will use $L = 144$, the 12th one. Traditionally, the Hofstadter model is distinguished by its butterfly-shaped energy spectrum with multi-fractal properties[48]. It also serves as an essential platform for investigating quantum Hall effects and Chern topological insulators[49,50].

Mirror-time symmetry breaking

The properties of system strongly depend on boundary conditions, and we first focus on the case under all PBCs (PBCs in both x and y dimensions). The Hamiltonian Eq.(1) possesses combined mirror-time (MT) symmetry as[28]

$$(\mathcal{MT})H(\mathcal{MT})^{-1} = H. \quad (2)$$

Operators of mirror reflection ($\mathcal{M}$) about the y-axis and time reversal ($\mathcal{T}$) are defined by $\mathcal{M}c_{n,m}\mathcal{M}^{-1} = c_{-n,m}$ and $\mathcal{T}i\mathcal{T}^{-1} = -i$ respectively. As a result, the energy spectrum can be either entirely real or composed of complex conjugate pairs. A real-to-complex spectral phase transition occurs along with the spontaneous breaking of the MT symmetry. To detect the MT symmetry breaking, in Fig. 1a we present the largest value of imaginary parts of all eigenenergies E, as a function of t_y. From now on, $t_x = 1$ is set as the energy unit. The MT symmetry breaking happens at $t_y = e^{-|g|}$ (dash line). When $t_y < e^{-|g|}$ the system is in the MT symmetry unbroken phase with a real spectrum, while the system is in the MT symmetry broken phase and the spectrum is complex when $t_y > e^{-|g|}$. To explore more features of the spectrum, in Fig. 1b we show typical spectra on the complex energy plane before and after the symmetry breaking. When $t_y < e^{-|g|}$, the spectrum is real without point-gap topology, and contains bands, each having subbands due to the fractal caused by quasiperiodicity[51]. Moreover, energy levels are highly degenerated with $2L$ degree of degeneracy (See Supplementary Note 1). When $t_y > e^{-|g|}$, the spectrum is complex with loops, which implies nontrivial spectral topologies. Energy levels are with L degree of degeneracy, and the lack of factor 2 is because of the broken MT symmetry.

The Hamiltonian Eq.(1) has translational symmetry in the y dimension and we can perform dimension reduction by conducting Fourier transformation in this dimension. It results in

$$H^x(k_y) = \sum_{n=1}^{L}[t_x c^\dagger_{n+1}c_n + h.c. + 2t_y\cos(2\pi\frac{F_l}{L}n - ig + \frac{k_y}{L}2\pi)c^\dagger_n c_n] \quad (3)$$

living in the x dimension, a 1D non-Hermitian Aubry-André-Harper (AAH) model[52,53]. In recent years, non-Hermitian AAH models have been extensively studied[54–56], focusing on Anderson localization and topology. Driven by the quasiperiodic potential (the last term in Eq.(3)), which acts as a quasirandom disorder, the model undergoes triple phase transitions at $t_y = e^{-|g|}$[56]. Due to the breaking of parity-time symmetry, which is similar to the MT symmetry, as t_y increases the spectrum turns from real to complex with loops, i.e., the phase transition of parity-time symmetry breaking. The emergence of loops also leads to a spectral topological phase transition. Furthermore, the spectrum is independent of the momentum k_y, which results in the L degree of degeneracy described above. The Hamiltonian remains the same, when we simultaneously add an integer k to k_y and shift the lattice index n to $n + n_0$ so that $\mathrm{mod}(F_l n_0, L) = L - k$. As for the eigenstates, they undergo an extended-localized phase transition. All states are extended when $t_y < e^{-|g|}$ while Anderson localized when $t_y > e^{-|g|}$. Localization lengths of states are energy- and k_y-independent, but localization centers are k_y-dependent and distributed all over the lattice. On the other hand, by performing the gauge transformation $c_{n,m} \to e^{i2\pi mn\beta}c_{n,m}$, we can rewrite the Hamiltonian Eq.(1) in another gauge $\mathbf{A} = (-\beta m, 0)$ (See Supplementary Note 2). The resulting Hamiltonian has translational symmetry in the x dimension. After performing dimension reduction, it leads to

$$H^y(k_x) = \sum_{m=1}^{L}\Big[t_y e^g c^\dagger_{m+1}c_m + t_y e^{-g}c^\dagger_m c_{m+1} + 2t_x\cos(2\pi\tfrac{F_l}{L}m - \tfrac{k_x}{L}2\pi)c^\dagger_m c_m\Big] \quad (4)$$

living in the y dimension, another non-Hermitian AAH model[57]. This Hamiltonian is independent of k_x. It has the same spectrum as H^x. Nevertheless, states have opposite localization properties: all states are Anderson localized when $t_y < e^{-|g|}$, while extended when $t_y > e^{-|g|}$.

Backing to the nonreciprocal Hofstadter model, we introduce spectral winding numbers[43,56]

$$\nu_p = \lim_{L\to\infty}\frac{1}{2\pi i}\int_0^{2\pi/L} dk_p \frac{\partial}{\partial k_p}\ln[\det(H(k_x, k_y))], \quad (5)$$

along x ($p = x$) and y ($p = y$) dimensions. They characterize how the spectral trajectory encircles the origin of the complex energy plane when the momentum k_p crosses the Brillouin zone. $H(k_x, k_y)$ is the Bloch Hamiltonian defined over the enlarged magnetic unit cell. It is equivalent to $H^x(k_y)$ with twisted boundary terms $[t_x e^{iLk_x}c^\dagger_1 c_L + h.c.]$. Analytical calculation shows that $\nu_x = 0$, indicating that the spectrum is topologically trivial in the x dimension (See Supplementary Note 3). But in the y dimension

$$\nu_y = \mathrm{sign}(g)\theta(t_y - e^{-|g|}), \quad (6)$$

with θ the step function. There is a topological phase transition, characterizing the presence of loops in the spectrum. On the other hand, known from the dimension reduction described above, the nonreciprocal Hofstadter model supports the directional localization of states[58]. Crucially, this is a global property of the entire band. When $t_y < e^{-|g|}$ all eigenstates are Anderson localized in the y dimension while extended in the x dimension, whereas they are extended in the y dimension while Anderson localized in the x dimension when $t_y > e^{-|g|}$ [see See Supplementary Note 5 for simulations]. The transition at $t_y = e^{-|g|}$ thus marks a collective switching of the localization direction for all eigenstates.

NHSE under all OBCs

Since we focus on NHSE without point-gap topology, we concentrate on the situation $t_y < e^{-|g|}$, where the spectrum under all PBCs is real and topologically trivial. Under all OBCs (OBCs in both x and y dimensions), we utilize

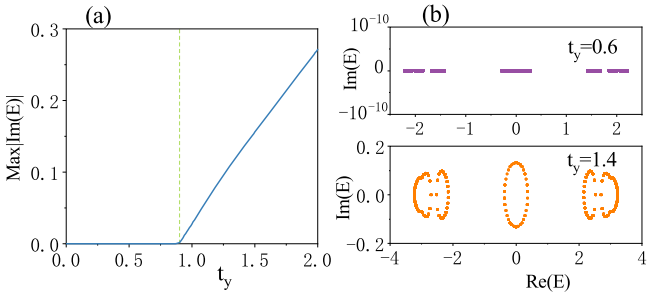

Fig. 1 | Mirror-time (MT) symmetry breaking. a The largest value of imaginary parts of all eigenenergies (Max|Im(E)|), as a function of t_y. **b** Spectra on the complex energy plane before ($t_y = 0.6$) and after ($t_y = 1.4$) the MT symmetry breaking. Systems are under periodic boundary conditions (PBCs) and with nonreciprocity $g = 0.1$.

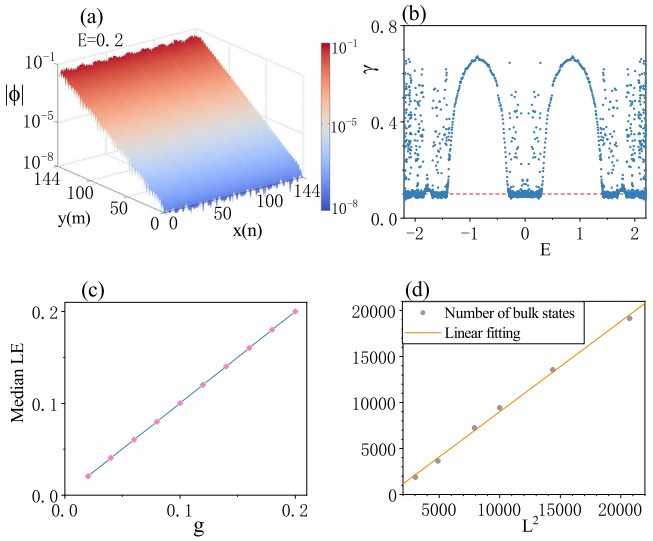

Fig. 2 | Non-Hermitian skin effect under open boundary conditions (OBCs). a Semi-log plot of the spatial distribution of the bulk eigenstate with energy $E = 0.2$. **b** Mean Lyapunov exponents (LEs) in the y dimension of all eigenstates, as a function of eigenenergy. The red dashed line indicates the value of nonreciprocity g. **c** Median LE of all eigenstates (LE of bulk eigenstates) versus the nonreciprocity g. **d** The number of bulk skin states versus the lattice size L^2. Systems are under all OBCs and with $g = 0.1$ and $t_y = 0.6$ if not specified.

the imaginary gauge transformation[59,60]

$$c_{n,m} = e^{gm} a_{n,m}, c^{\dagger}_{n,m} = e^{-gm} \widetilde{a}_{n,m}. \quad (7)$$

$a(\widetilde{a})$ is the annihilation (creation) operator, but $\widetilde{a}$ is not the Hermitian conjugate of a. We transform the Hamiltonian Eq.(1) into the same form but without the nonreciprocal hopping ($g = 0$). Thus, the model has the same real spectrum as the Hermitian Hofstadter model. The above degeneracy of $2L$ degrees is broken! (See Supplementary Note 1)

As for eigenstates, we present the spatial distribution of a typical bulk one in Fig. 2a. All bulk states are exponentially localized at the large (small) y edge when $g > (<) 0$, exceptionally showing NHSE. To quantitatively study NHSE, we adopt the exponential wave function $\phi_{n,m} = f(n)e^{\mathrm{sign}(g)\gamma_n m}$, where γ_n are Lyapunov exponents (LEs or inverse of localization lengths) in the y dimension. Fitting eigenstates with the above wave function, we extract mean LEs $\gamma = \sum_n \gamma_n / L$ and mean squared errors of the LEs, summing over the lattice index n (in the x dimension). In Fig. 2b we present mean LEs, as a function of eigenenergy, of all eigenstates for a system with $t_y < e^{-|g|}$. Compared to Fig. 1b, states emerge in gaps, whose mean LEs and mean squared errors are larger than that of majority states (See also Supplementary Note 4). These are edge states caused by the Chern topological nature of the nonreciprocal Hofstadter model[61]. On the other hand, the majority states, which are bulk states, have approximately the same mean LE. To obtain the LE of these bulk states, we extract the median LE $\overline{\gamma}$ over all eigenstates. In Fig. 2c we show its relation with the nonreciprocity g. The LE of bulk states $\overline{\gamma} = |g|$, independent of other parameters. Furthermore, we count the number of eigenstates whose mean LEs lie in the interval $\overline{\gamma} \times [1 - \varepsilon, 1 + \varepsilon]$ with a small $\varepsilon = 0.1$, considering it the number of bulk states. We present the number versus the lattice size L^2 in Fig. 2d. It is fitted by a straight line with the slope 98%, which can be seen as the proportion of bulk states. The linear relation further indicates that the NHSE in the nonreciprocal Hofstadter model is of the first order, where an extensive number $\mathcal{O}(L^d)$ of skin modes emerge in a d dimensional system[62–64].

Open-boundary-induced degeneracy breaking

To explain the mechanism behind, we start from the case under all PBCs and open the boundaries in the y and x dimensions successively. Numerical simulations under various boundary conditions are presented in the Supplementary Note 5. From above, we know that when $t_y < e^{-|g|}$ the system supports directional localization of states under all PBCs. Eigenstates are extended in the x dimension and Anderson localized in the y dimension. Like in nonreciprocal AAH models[57], the localization of states in the y dimension suppresses the effects of nonreciprocity and leads to a real spectrum. Furthermore, for AAH models in the Anderson localized phase, bulk eigenstates are exponentially localized in the bulk, which makes them independent of boundary conditions[57,65]. Correspondingly, when $t_y < e^{-|g|}$ and under all PBCs, eigenstates are exponentially localized in the y dimension while extended in the x dimension. Then, the localization and energies of bulk states remain the same when we turn the PBC into OBC in the y dimension (y-PBC into y-OBC). Except for the emergence of edge states in gaps, which is not the focus here, the degeneracy of bulk states is approximately the same, and the reality of bulk spectrum still holds. Things are different when we change x-PBC to x-OBC.

Under y-OBC, the above-introduced imaginary gauge transformation works regardless of the boundary condition in the x dimension. Note that it does not work under y-PBC. The nonreciprocal and the Hermitian Hofstadter models share the same spectrum, when under y-OBC and the same boundary condition in the x dimension. A correspondence can be made through the transformation, between the right eigenstates of two models. Given that $\varphi_{n,m}$ is an eigenstate of the Hermitian Hofstadter model under y-OBC and x-PBC(OBC), $\phi_{n,m} = e^{gm}\varphi_{n,m}$ is a right eigenstate of the nonreciprocal model under y-OBC and x-PBC(OBC). It clearly shows how nonreciprocal hopping affects states in different phases. For states of the Hermitian Hofstadter model, which are extended in the y dimension, corresponding wave functions $\phi_{n,m}$ are exponentially localized at the large (small) y edge when $g > (<) 0$. This works for the case under all OBCs, and the resulting states are skin states with LEs $\gamma = |g|$. For Anderson localized bulk eigenstates of the Hermitian Hofstadter model, wave functions $\phi_{n,m}$ are also Anderson localized in the y dimensional bulk but with different right and left side LEs (the case under y-OBC and x-PBC).

Through the imaginary gauge transformation, we obtain that when $t_y < e^{-|g|}$ and under y-OBC and x-PBC, the spectrum of the Hermitian Hofstadter model has huge degeneracy. Moreover, bulk states of the Hermitian Hofstadter model are Anderson localized in the y dimensional bulk while extended in the x dimension. We choose that eigenstates have translational symmetry along the x direction, and the momentum k_x is a good quantum number. Supposing that an eigenstate $|\varphi\rangle$ of energy E has a momentum k_x in the x dimension and is exponentially localized around m_0 in the y dimensional bulk, we can obtain new states that have the same energy E and construct the corresponding degenerate subspace. Easily seen in the dimension-reduced Hamiltonian $H^y(k_x)$, when we add an integer k to the momentum k_x, the Hamiltonian remains the same, by shifting the lattice index m to $m + m_1$ so that $\mathrm{mod}(F_l m_1, L) = k$ and emerging phases in the cosine function cancel. New states in the degenerate subspace are obtained by performing the same operation on the state $|\varphi\rangle$, as long as they are localized in the y dimensional bulk. Furthermore, the state with momentum

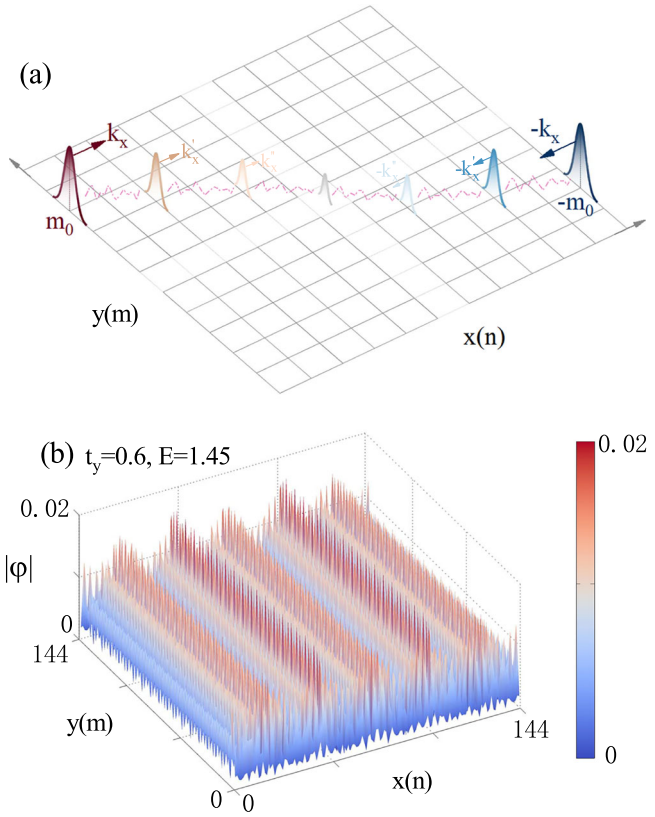

Fig. 3 | Open-boundary-induced degeneracy breaking. For the Hermitian Hofstadter model, degenerated bulk eigenstates under x-PBC, which are localized in the y dimensional bulk and extended in the x dimension, have to superpose together to meet the need of x-OBC (schematically shown in (**a**)). **b** Spatial distribution of the bulk eigenstate with energy $E = 1.45$, for the system under all OBCs and with $g = 0$ and $t_y = 0.6$.

Table 1 | Summary of the spectral and bulk eigenstate properties for the nonreciprocal Hofstadter model with $t_y < e^{-|g|}$ under different boundary conditions

All PBCs	Spectrum: real, $2L$-degeneracy States: x-extended, y-Anderson-localized
x-PBC & y-OBC	Spectrum: real, ~ $2L$-degeneracy States: x-extended, y-Anderson-localized
x-OBC & y-PBC	Spectrum: real for bulk states, no degeneracy States: extended in both dimensions
All OBCs	Spectrum: real, no degeneracy States: x-extended, y-skin-localized

$-k_x$ and being localized around $-m_0$ is also in the degenerate subspace, ensured by the MT symmetry. All these states contribute the approximate $2L$ degree of degeneracy.

Now, we further change the x-PBC into x-OBC. This is the pivotal step that induces the NHSE. To meet the need of x-OBC, the state with energy E and momentum k_x has to superpose with the state which has the same energy E but opposite momentum $-k_x$ to form a standing wave in the x dimension. However, these two states are spatially separated in the y dimension, which makes the superposition impossible [see Fig. 3a]. To bridge these two states to satisfy the x-OBC, all bulk states in the degenerate subspace, being Anderson localized at different positions in the y dimension and having different momenta k_x, must superpose together. This superposition across the degenerate subspace breaks the degeneracy and hybridizes the y-localized states into states that are extended in both dimensions [see Fig. 3b]. However, the essences of the "extended" in x and y dimensions are different, which will be shown later. Finally, through the imaginary gauge transformation again, we know that under all OBCs, all bulk eigenstates of the nonreciprocal Hofstadter model are skin states with LEs $\gamma = |g|$, which explains the median LE. For reference, we summarize in Table 1 the properties of the spectrum and bulk eigenstates under different boundary conditions. Further details are provided in Supplementary Notes 1 and 4–6.

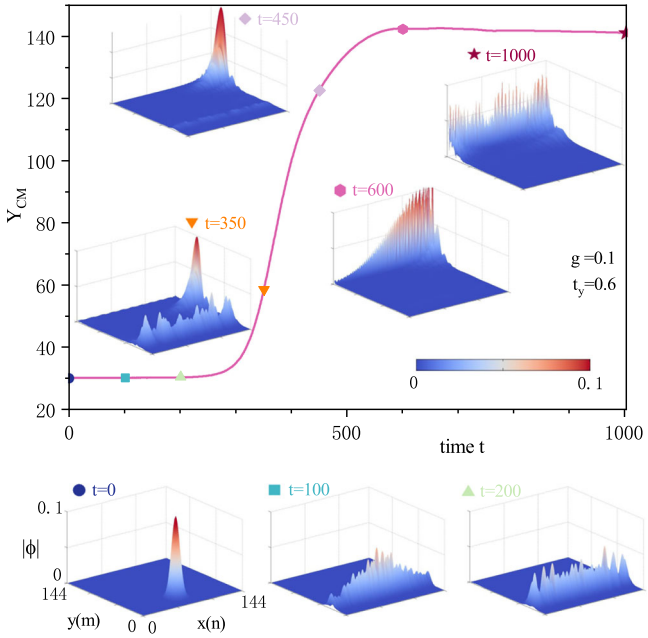

Fig. 4 | Anomalous wave packet dynamics. Time evolution of the center of mass Y_{CM}, in the dynamics of an initial Gaussian wave packet on the lattice under all OBCs and with nonreciprocity $g = 0.1$ and $t_y = 0.6$. Besides, spatial distributions of the wave packet at specific times are also presented. The dynamics show anisotropic bulk transport and directional edge flow.

Anomalous wave packet dynamics

Not only the spectrum and eigenstates, but the NHSE also significantly affects several dynamic properties of the system even in bulk. The appearance of a directional (chiral) bulk flow is a typical phenomenon[17,66]. We simulate the time evolution of a wave packet, which is initially in the Gaussian form $|\phi_0\rangle = \mathcal{N}\sum_{n,m}\exp[-(n-n_0)^2/25-(m-m_0)^2/25]c^\dagger_{n,m}|0\rangle$. Here, $\mathcal{N}$ is the normalization factor, and $n_0 = 70$, $m_0 = 30$ are coordinates of the center of the initial wave packet. Let us indicate by Y_{CM} the center of mass in the y dimension of the wave packet. It is given by the normalized expectation value of the position operator

$$Y_{CM}(t) = \langle\phi(t)|\sum_{n,m} m c^\dagger_{n,m}c_{n,m}|\phi(t)\rangle. \tag{8}$$

In Fig. 4 we present the time evolution of Y_{CM} for the system under all OBCs and with $t_y < e^{-|g|}$, while the one for $t_y > e^{-|g|}$ is shown in Supplementary Note 7. In the directional bulk flow caused by normal NHSE, the center of mass increases linearly with time in the Lieb-Robinson velocity[67]. In contrast, here, Y_{CM} is constant in the beginning, followed by a rapid increase to the maximum. Finally, the wave packet accumulates at the large y edge, showing NHSE.

To investigate the physics behind the anomalous directional flow, we further present in Fig. 4 spatial distributions of normalized states $|\phi(t)\rangle = \mathcal{N}(t)e^{-iHt}|\phi_0\rangle$ at specific times. Initially, the wave packet only expands in the x dimension, and the center of mass in the y dimension keeps constant. Bulk eigenstates under all OBCs are skin states that are localized in the y dimensional edge, but they are superpositions of states that are Anderson

localized in the y dimensional bulk, while they are extended in the x dimension. The system has an anisotropic conductivity with vanishing bulk transport in the y dimension[68], because of the directional Anderson localized nature of states. When the wave packet expands to the edges, chiral edge states start to play roles, due to the non-orthogonality of states in non-Hermitian systems. These edge states result from the Chern topological nature of the nonreciprocal Hofstadter model, and they are ballistic along edges. NHSE of the chiral edge states forces the wave packet to move along the edge to the top-right corner, and correspondingly, the center of mass in the y dimension increases dramatically. After expanding in the large y edge, which does not cause apparent changes in Y_{CM}, the wave packet finally evolves into a skin state.

Conclusion and discussion

We have reported NHSE without point-gap topology in the 2D nonreciprocal Hofstadter model. It results from the OBC-induced degeneracy breaking and manifests an anomalous directional flow of wave packet. Techniques to generate (artificial) magnetic fields have been well established in various candidate non-Hermitian systems, such as ultra-cold atoms[69], photonic and acoustic structures[70,71], and electric circuits[72], where the NHSE has been observed[17,31,73,74]. Thus, the physics shown above is highly accessible in experiments. For example, in electric circuits, the single-particle problem can be simulated by Kirchhoff's current law $I_a(\omega) = \sum_{b=1}^{L} J_{ab}(\omega) V_b(\omega)$, where the Laplacian J of the circuit acts as the effective Hamiltonian, and I_a and V_a are the current and voltage at node a. Periodic arrays of capacitors and inductors are known to simulate the physics in crystal lattices[75]. Nonreciprocal hopping amplitudes are realized by negative impedance converters with current inversion (INICs)[76]. Artificial magnetic fields are generated by spatially varying electric elements[72]. Further studies on (higher-order) NHSE and topology in highly degenerated systems, such as Moiré materials, systems with flat bands, and (artificial) magnetic lattices, will be interesting.

Methods

The eigenenergies and eigenstates are obtained by performing exact diagonalization of the non-Hermitian, non-interacting Hamiltonian, $H|\phi_i\rangle = E_i|\phi_i\rangle$, where $|\phi_i\rangle$ denotes the i-th right eigenstate. The spatial distribution (wavefunction) of an eigenstate is given by $\phi^i_{n,m} = \langle n, m|\phi_i\rangle$, with $\langle n, m|$ representing the Wannier state localized at lattice site (n, m). For the time evolution of a wave packet, $|\phi(t)\rangle = e^{-iHt}|\phi_0\rangle$, we numerically compute the action of the matrix exponential e^{-iHt} on the initial state vector $|\phi_0\rangle$. The resulting state is then normalized such that $\langle\phi(t)|\phi(t)\rangle = 1$.

Data availability

The numerical data presented in the figures are available at https://doi.org/10.5281/zenodo.18065332. Further raw data are also available from the author upon request.

Code availability

The source codes we have tailored and employed are also available at https://doi.org/10.5281/zenodo.18065332.

Received: 24 July 2025; Accepted: 6 January 2026;
Published online: 14 January 2026

References

1. Bender, C. M. & Boettcher, S. Real spectra in non-Hermitian Hamiltonians having $\mathcal{PT}$ symmetry. *Phys. Rev. Lett.* **80**, 5243 (1998).
2. Bender, C. M. Making sense of non-Hermitian Hamiltonians. *Rep. Prog. Phys.* **70**, 947 (2007).
3. Ashida, Y., Gong, Z. & Ueda, M. Non-Hermitian physics. *Adv. Phys.* **69**, 249 (2020).
4. Tang, W. et al. Exceptional nexus with a hybrid topological invariant. *Science* **370**, 1077 (2020).
5. Ding, K., Ma, G., Zhang, Z. Q. & Chan, C. T. Experimental demonstration of an anisotropic exceptional point. *Phys. Rev. Lett.* **121**, 085702 (2018).
6. Zhang, Q. et al. Observation of acoustic non-Hermitian Bloch braids and associated topological phase transitions. *Phys. Rev. Lett.* **130**, 017201 (2023).
7. Tang, W., Ding, K. & Ma, G. Experimental realization of non-Abelian permutations in a three-state non-Hermitian system. *Natl. Sci. Rev.* **9**, nwac010 (2022).
8. Ding, K., Ma, G., Xiao, M., Zhang, Z. Q. & Chan, C. T. Emergence, coalescence, and topological properties of multiple exceptional points and their experimental realization. *Phys. Rev. X* **6**, 021007 (2016).
9. Ozawa, T. et al. Topological photonics. *Rev. Mod. Phys.* **91**, 015006 (2019).
10. Feng, L., El-Ganainy, R. & Ge, L. Non-Hermitian photonics based on parity-time symmetry. *Nat. Photonics* **11**, 752 (2017).
11. Regensburger, A. et al. Parity-time synthetic photonic lattices. *Nat. (Lond.)* **488**, 167 (2012).
12. Feng, L., Wong, Z. J., Ma, R.-M., Wang, Y. & Zhang, X. Single-mode laser by parity-time symmetry breaking. *Science* **346**, 972 (2014).
13. Zhen, B. et al. Spawning rings of exceptional points out of Dirac cones. *Nat. (Lond.)* **525**, 354 (2015).
14. Zhou, H. et al. Observation of bulk Fermi arc and polarization half charge from paired exceptional points. *Science* **359**, 1009 (2018).
15. Bandres, M. A. et al. Topological insulator laser: Experiments. *Science* **359**, eaar4005 (2018).
16. Malzard, S., Poli, C. & Schomerus, H. Topologically protected defect states in open photonic systems with non-Hermitian charge-conjugation and parity-time symmetry. *Phys. Rev. Lett.* **115**, 200402 (2015).
17. Liang, Q. et al. Dynamic signatures of non-Hermitian skin effect and topology in ultracold atoms. *Phys. Rev. Lett.* **129**, 070401 (2022).
18. Ren, Z. et al. Chiral control of quantum states in non-Hermitian spin-orbit-coupled fermions. *Nat. Phys.* **18**, 385 (2022).
19. Shen, H. & Fu, L. Quantum oscillation from in-gap states and a non-Hermitian Landau level problem. *Phys. Rev. Lett.* **121**, 026403 (2018).
20. Yoshida, T., Peters, R. & Kawakami, N. Non-Hermitian perspective of the band structure in heavy-fermion systems. *Phys. Rev. B* **98**, 035141 (2018).
21. Buddhiraju, S., Song, A., Papadakis, G. T. & Fan, S. Nonreciprocal metamaterial obeying time-reversal symmetry. *Phys. Rev. Lett.* **124**, 257403 (2020).
22. Chen, W., Özdemir, S. K., Zhao, G., Wiersig, J. & Yang, L. Exceptional points enhance sensing in an optical microcavity. *Nature* **548**, 192 (2017).
23. Peng, B. et al. Chiral modes and directional lasing at exceptional points. *Proc. Natl. Acad. Sci.* **113**, 6845 (2016).
24. Konotop, V. V., Yang, J. & Zezyulin, D. A. Nonlinear waves in $\mathcal{PT}$-symmetric systems. *Rev. Mod. Phys.* **88**, 035002 (2016).
25. El-Ganainy, R. et al. Non-Hermitian physics and PT symmetry. *Nat. Phys.* **14**, 11 (2018).
26. Lee, T. E. Anomalous edge state in a non-Hermitian lattice. *Phys. Rev. Lett.* **116**, 133903 (2016).
27. Yao, S. & Wang, Z. Edge states and topological invariants of non-Hermitian systems. *Phys. Rev. Lett.* **121**, 086803 (2018).
28. Zhang, X., Zhang, T., Lu, M.-H. & Chen, Y.-F. A review on non-Hermitian skin effect. *Adv. Phys.: X,* **7**, 2109431 (2022).
29. Lin, R., Tai, T., Li, L. & Lee, C. H. Topological non-Hermitian skin effect. *Front. Phys.* **18**, 53605 (2023).
30. McDonald, A. & Clerk, A. A. Exponentially-enhanced quantum sensing with non-Hermitian lattice dynamics. *Nat. Commun.* **11**, 5382 (2020).
31. Weidemann, S. et al. Topological funneling of light. *Science* **368**, 311 (2020).
32. Xue, W.-T., Hu, Y.-M., Song, F. & Wang, Z. Non-Hermitian edge burst. *Phys. Rev. Lett.* **128**, 120401 (2022).

33. Lee, C.-H. & Longhi, S. Ultrafast and anharmonic Rabi oscillations between non-Bloch bands. *Commun. Phys.* **3**, 147 (2020).
34. Budich, J. C. & Bergholtz, E. J. Non-Hermitian topological sensors. *Phys. Rev. Lett.* **125**, 180403. (2020).
35. Yuan, H. et al. Non-Hermitian topolectrical circuit sensor with high sensitivity. *Adv. Sci.* **10**, 2301128 (2023).
36. Kunst, F. K., Edvardsson, E., Budich, J. C. & Bergholtz, E. J. Biorthogonal bulk-boundary correspondence in non-Hermitian systems. *Phys. Rev. Lett.* **121**, 026808 (2018).
37. Yang, Z., Zhang, K., Fang, C. & Hu, J. Non-Hermitian bulk-boundary correspondence and auxiliary generalized Brillouin zone theory. *Phys. Rev. Lett.* **125**, 226402 (2020).
38. Kawabata, K., Numasawa, T. & Ryu, S. Entanglement phase transition induced by the non-Hermitian skin effect. *Phys. Rev. X* **13**, 021007 (2023).
39. Okuma, N., Kawabata, K., Shiozaki, K. & Sato, M. Topological origin of non-Hermitian skin effects. *Phys. Rev. Lett.* **124**, 086801 (2020).
40. Wang, H.-Y., Song, F. & Wang, Z. Amoeba formulation of non-Bloch band theory in arbitrary dimensions. *Phys. Rev. X* **14**, 021011 (2024).
41. Hu, H. Topological origin of non-Hermitian skin effect in higher dimensions and uniform spectra, Science Bulletin, https://doi.org/10.1016/j.scib.2024.07.022
42. Zhang, K., Fang, C. & Yang, Z. Dynamical degeneracy splitting and directional invisibility in non-Hermitian systems. *Phys. Rev. Lett.* **131**, 036402 (2023).
43. Zhang, K., Yang, Z. & Fang, C. Universal non-Hermitian skin effect in two and higher dimensions. *Nat. Commun.* **13**, 2496 (2022).
44. Zak, J. Magnetic translation group. *Phys. Rev.* **134**, A1602 (1964).
45. Lu, M., Zhang, X.-X. & Franz, M. Magnetic suppression of non-Hermitian skin effects. *Phys. Rev. Lett.* **127**, 256402 (2021).
46. Shao, K., Cai, Z.-T., Geng, H., Chen, W. & Xing, D. Y. Cyclotron quantization and mirror-time transition on nonreciprocal lattices. *Phys. Rev. B* **106**, L081402 (2022).
47. Szabó, A. & Schneider, U. Non-power-law universality in one-dimensional quasicrystals. *Phys. Rev. B* **98**, 134201 (2018).
48. Hofstadter, D. R. Energy levels and wave functions of Bloch electrons in rational and irrational magnetic fields. *Phys. Rev. B* **14**, 2239 (1976).
49. Thouless, D. J., Kohmoto, M., Nightingale, M. P. & den Nijs, M. Quantized Hall conductance in a two-dimensional periodic potential. *Phys. Rev. Lett.* **49**, 405 (1982).
50. Shen, H., Zhen, B. & Fu, L. Topological band theory for non-Hermitian Hamiltonians. *Phys. Rev. Lett.* **120**, 146402 (2018).
51. He, Z., Guo, X.-Y., Ma, Z. & Gao, J.-H. Energy spectrum theory of incommensurate systems. *Natl. Sci. Rev.* **11**, nwae083 (2024).
52. Aubry, S. & André, G. Analyticity breaking and Anderson localization in incommensurate lattices. *Ann. Isr. Phys. Soc.* **3**, 133 (1980).
53. Harper, P. G. Single band motion of conduction electrons in a uniform magnetic field. *Proc. Phys. Soc., Lond., Sect. A* **68**, 874 (1955).
54. Weidemann, S., Kremer, M., Longhi, S. & Szameit, A. Topological triple phase transition in non-Hermitian Floquet quasicrystals. *Nature* **601**, 354 (2022).
55. Lin, Q. et al. Topological phase transitions and mobility edges in non-Hermitian quasicrystals. *Phys. Rev. Lett.* **129**, 113601 (2022).
56. Longhi, S. Topological phase transition in non-Hermitian quasicrystals. *Phys. Rev. Lett.* **122**, 237601 (2019).
57. Jiang, H., Lang, L.-J., Yang, C., Zhu, S.-L. & Chen, S. Interplay of non-Hermitian skin effects and Anderson localization in nonreciprocal quasiperiodic lattices. *Phys. Rev. B* **100**, 054301 (2019).
58. Paul, N., Crowley, P. J. D. & Fu, L. Directional localization from a magnetic field in Moiré systems. *Phys. Rev. Lett.* **132**, 246402 (2024).
59. Rivero, J. H. D., Feng, L. & Ge, L. Imaginary gauge transformation in momentum space and Dirac exceptional point. *Phys. Rev. Lett.* **129**, 243901 (2022).
60. Qi, Y. et al. Extended imaginary gauge transformation in a general nonreciprocal lattice. *Phys. Rev. B* **110**, 075411 (2024).
61. Yao, S., Song, F. & Wang, Z. Non-Hermitian Chern bands. *Phys. Rev. Lett.* **121**, 136802 (2018).
62. Kawabata, K., Sato, M. & Shiozaki, K. Higher-order non-Hermitian skin effect. *Phys. Rev. B* **102**, 205118 (2020).
63. Zhang, X., Tian, Y., Jiang, J.-H., Lu, M.-H. & Chen, Y.-F. Observation of higher-order non-Hermitian skin effect. *Nat. Commun.* **12**, 5377 (2021).
64. Lee, C. H., Li, L. & Gong, J. Hybrid higher-order skin-topological modes in nonreciprocal systems. *Phys. Rev. Lett.* **123**, 016805 (2019).
65. Cai, X. Boundary-dependent self-dualities, winding numbers, and asymmetrical localization in non-Hermitian aperiodic one-dimensional models. *Phys. Rev. B* **103**, 014201 (2021).
66. Li, Z. et al. Observation of dynamic non-Hermitian skin effects. *Nat. Commun.* **15**, 6544 (2024).
67. Gong, Z. et al. Topological phases of non-Hermitian systems. *Phys. Rev. X* **8**, 031079 (2018).
68. Poon, T.-F. J., Wan, Y., Wang, Y. & Liu, X.-J. Anomalous universal quantum transport in a two-dimensional asymptotic quasiperiodic system. *Phys. Rev. B* **111**, L220204 (2025).
69. Lin, Y.-J., Compton, R. L., Jiménez-García, K., Porto, J. V. & Spielman, I. B. Synthetic magnetic fields for ultracold neutral atoms. *Nat. (Lond.)* **462**, 628 (2009).
70. Lumer, Y. et al. Light guiding by artificial gauge fields. *Nat. Photonics* **13**, 339 (2019).
71. Wen, X. et al. Acoustic Landau quantization and quantum-Hall-like edge states. *Nat. Phys.* **15**, 352 (2019).
72. Zhang, X.-X. & Franz, M. Non-Hermitian exceptional Landau quantization in electric circuits. *Phys. Rev. Lett.* **124**, 046401 (2020).
73. Zhang, L. et al. Acoustic non-Hermitian skin effect from twisted winding topology. *Nat. Commun.* **12**, 6297 (2021).
74. Liu, S. et al. Non-Hermitian skin effect in a non-Hermitian electrical circuit. *Res. (Wash. D.C.)* **2021**, 5608038 (2021).
75. Dong, J., Juričić, V. & Roy, B. Topolectric circuits: Theory and construction. *Phys. Rev. Res.* **3**, 023056 (2021).
76. Hofmann, T., Helbig, T., Lee, C. H., Greiter, M. & Thomale, R. Chiral voltage propagation and calibration in a topolectrical Chern circuit. *Phys. Rev. Lett.* **122**, 247702 (2019).

Acknowledgements

This work is supported by the Quantum Science and Technology-National Science and Technology Major Project under grant No. 2023ZD0300400, the Natural Science Foundation of Hubei Province under grant No. 2022CFB272, and the National Natural Science Foundation of China under grant No. 12134015 and No. 12175290.

Author contributions

This work was completed by Xiaoming Cai alone.

Competing interests

The authors declare no competing interests.

Additional information

Supplementary information The online version contains supplementary material available at https://doi.org/10.1038/s42005-026-02496-9.

Correspondence and requests for materials should be addressed to Xiaoming Cai.

Peer review information *Communications Physics* thanks Zhoutao Lei and the other, anonymous, reviewer(s) for their contribution to the peer review of this work. [A peer review file is available].